Oxford Open Materials Science, 2023, **3(1)**, itad014
https://doi.org/10.1093/oxfmat/itad014
Research article

Lacunarity as a quantitative measure of mixing—a micro-CT analysis-based case study on granular materials

Lívia Vásárhelyi [1], Dániel Sebők [1], Imre Szenti[1], Ádám Tóth[1], Sára Lévay[2,3], Róbert Vajtai [4], Zoltán Kónya[1,5] Ákos Kukovecz[1,*]

[1]Interdisciplinary Excellence Centre, Department of Applied and Environmental Chemistry, University of Szeged, H-6720, Rerrich Béla tér 1, Szeged, Hungary
[2]University of Lyon, INSA-Lyon, CNRS UMR5259, LaMCoS, 69621 Villeurbanne, France
[3]Institute for Solid State Physics and Optics, Wigner Research Centre for Physics, Budapest H-1121, Hungary
[4]Department of Materials Science and Nanoengineering, Rice University, Houston, TX MS 325, USA
[5]ELKH-SZTE Reaction Kinetics and Surface Chemistry Research Group, H-6720 Szeged Rerrich Béla tér 1, Hungary

*Correspondence address: Interdisciplinary Excellence Centre, Department of Applied and Environmental Chemistry, University of Szeged, H-6720, Rerrich Béla tér 1, Szeged, Hungary; Tel: +3662343491; Email: kakos@chem.u-szeged.hu.

Abstract

In practically every industry, mixing is a fundamental process, yet its 3D analysis is scarce in the literature. High-resolution computed tomography (micro-CT) is the perfect X-ray imaging tool to investigate the mixing of granular materials. Other than qualitative analysis, 3D micro-CT images provide an opportunity for quantitative analysis, which is of utmost importance, in terms of efficiency (time and budget) and environmental impact of the mixing process. In this work, lacunarity is proposed as a measure of mixing. By the lacunarity calculation on the repeated micro-CT measurements, a temporal description of the mixing can be given in three dimensions. As opposed to traditional mixing indices, the lacunarity curve provides additional information regarding the spatial distribution of the grains. Discrete element method simulations were also performed and showed similar results to the experiments.

Keywords: lacunarity; micro-CT; mixing; granular materials; spatial heterogeneity; DEM simulations

Introduction

Mixing is a fundamental part of our everyday life and practically in every industry. We mix everything from liquids to powders and granular materials. It is one of the most basic processes, yet very complex; the more we study it, the more complex it seems. The driving forces, the containers, the mixed materials, their interactions, density, speed, mixing time and plenty of other factors all affect the mixing efficiency. Some of the most important industrial applications are in the fields of food chemistry [1, 2], construction [3, 4], pharmaceuticals [5, 6], cosmetics [7] and materials science [8, 9]. By definition, mixing is the process of causing a flow inside a heterogeneous system to disperse its components as evenly as possible. Uneven mixing can cause various problems; thus, it is exceptionally important to be able to quantify the goodness of mixing, or, in other words, the homogeneity of the mixture. Overmixing, on an industrial scale, can cause huge energy waste, thus increasing manufacturing costs unnecessarily. Under-mixing could even cause potentially fatal problems; for example, if the compounds of a drug do not get homogeneously mixed, this can result in pills without the correct amount of active ingredients [10, 11]. Furthermore, it is well known that agitated granular mixtures tend to spontaneous segregation [12] in many situations. Opposed to under-mixing, segregation can result in the complete separation of ingredients based on their size, shape, surface, density, etc. However, it also holds the potential for applications when demixing is intended, but it has an undesired side effect in our case when the goal is to obtain perfectly mixed samples.

Even though the segregation and mixing of granular materials have been studied for decades, we can state that it is still an imperfectly understood phenomenon. A fundamental understanding is still lacking, despite its potentially beneficial impact on several industries. Therefore, the precise evaluation, visualization and quantification of the (de)mixing process are of utmost importance. Several different mechanisms have been suggested to explain the phenomena using experimental techniques (such as velocimetric, spectroscopic and tomographic), and different simulation approaches (such as particle level and continuum) [13–21], just to mention a few.

Computed tomography (CT) is an X-ray imaging method originally developed for medical purposes [22]. With technological advancement, high (even submicron) resolutions became achievable and high-resolution CT (micro-CT) was born [23]. It is a non-destructive 3D imaging tool based on the different X-ray attenuation of materials (mainly influenced by density and chemical composition), which nowadays is widely used in materials science [24]. During the measurement, samples are placed on a rotating sample holder and hundreds or thousands of X-ray images are taken from different angles, the original 3D structure

Received: March 31, 2023. **Revised:** July 5, 2023. **Accepted:** July 24, 2023

of materials can be reconstructed by computer. The non-destructive nature of the technique allows for conducting temporal investigations [25]. The same sample can be examined at different times while exposed to various effects. Individual granules can be followed during the process and their trajectory can be determined during mixing. By using specific testing stages, in situ measurements can be conducted, even close to real time. Although the technique is perfect for visualizing the mixing process, there are only a few examples in the scientific literature of micro-CT used for this purpose [15, 26, 27]. Liu *et al.* used synchrotron micro-CT to investigate the mixing and segregation of granular matter. They examined the mixture homogeneity after a number of rotations and quantified it using a mixing index. They found that fewer spherical granules moved to the top of the mixture [28].

Lacunarity is a descriptor of spatial heterogeneity and deviation from translational homogeneity, which was first presented by Mandelbrot as a complement of fractal dimension [29]. In general, lacunarity is represented as a function of box size (as opposed to a single numerical value), and the shape of the curve carries additional information [30, 31]. Higher lacunarity values mean a higher level of heterogeneity at a given box size; with increasing box size, the lacunarity tends to decrease. The absolute value of lacunarity is dependent on the density of the binary images, thus comparison of different samples is easier after normalization.

Lacunarity has widespread applications in many scientific fields from medicine [32, 33, 34], through bioengineering [35, 36] to geology [37–39]. It is a valuable descriptor of the spatial heterogeneity of pores, for example in soils [38] and granular materials [40]. A huge benefit of lacunarity is that it can be calculated not only in 2D but also in 3D, and thus can be used to quantify the spatial heterogeneity on 3D (micro-)CT images. Xia *et al.* [37] calculated the lacunarity of pores in reservoir rocks to use in permeability predictions based on micro-CT images, whereas dos Santos *et al.* [38] used lacunarity to describe the void space of soils in micro-CT images. There are a few examples of lacunarity calculations for quantifying the mixing efficiency. Pennella *et al.* used lacunarity for the quantification of fluid particle dispersion and to describe the overall mixing efficiency, but only in 2D [41].

The traditional computational method is called the gliding box method (GBM) [42, 43], which provides reliable and detailed results, but its calculation for real-life 3D micro-CT datasets takes an exceptionally long time, thus it is not practical for everyday use. Our calculation method (called the fixed-grid method, FGM) described in a previous publication provides reliable results in 3D in a fraction of the computational time of GBM. The details of the FGM and the reliability of the calculations were presented there [44]. The main idea behind the FGM is to drastically decrease the number of boxes in the calculations. As opposed to the GBM, where lacunarity is calculated for overlapping boxes, FGM only uses non-overlapping boxes, while the calculation method remains the same. The lacunarity is calculated for binary images based on the first and second moments of the probability distribution of the box masses. The real effect of this seemingly small change can be seen in the case of real-life 3D micro-CT datasets, where the number of boxes decreases with several orders of magnitude (e.g. for a 800 × 800 × 800 voxel dataset, the GBM calculates the masses of 423 564 751 boxes with 50 voxel side lengths, while FGM only uses 4096) [44].

Lacunarity is not only valuable for real-life experiments but can also be calculated for simulated datasets [40, 45]. Mixing can somewhat easily be modeled by discrete element methods (DEM) [21, 46–48], which examines the particle interactions on a scale comparable to the size of the particles. Given the overly complex nature of interactions and deformations in real-life systems, in DEM models, the assumption is that the particles are spherical and non-deformable and they can overlap. The simulations of mixing are extensively studied in the literature. It can be used to simulate mixing in various mixers under diverse conditions [49–54]. Lévay *et al.* used DEM simulations to model the behavior of spherical particles as a result of shaking [55, 56]. It is quite obvious that DEM is a valuable tool for investigating mixing, and by calculating lacunarity, the results of the simulations can be directly compared with real-life datasets (e.g. micro-CT), thus lacunarity can be the common ground between simulated and experimental data.

Quantification of mixing efficiency is without a doubt an important task, and there are several existing mixing indices available [57–63]. Mixing indices can be sorted into two categories [64]. The first one uses statistical data based on a sampling of the system to determine the state of mixing [65, 66], which carries a disadvantage within itself, namely the index can vary depending on sampling size and conditions. The other type, however, uses data from all the particles in the system [67–69], which has the potential of becoming very time-consuming. A good mixing index should fulfill several requirements: it should be dimensionless; its values should be between 0 and 1 (where 0 means no mixing and 1 means completely homogeneous mixing); and the values should increase linearly with increasing homogeneity. Non-sampling mixing index (SMI) is, in a sense, similar to lacunarity since it calculates for subdomains first, and then gives a cumulative result [64]. SMI is not a statistical type mixing index; instead, it uses local mixing information and integrates the data of the subdomains into the whole system. Traditional mixing indices provide a single value to describe the state of a mixture, which is an advantage for comparative purposes. Although lacunarity curves cannot be directly compared with mixing indices, one of their greatest strengths is the fact that they provide additional information regarding the structure of the system (e.g. the granule size can be estimated based on the curve [30]).

Here, we present lacunarity calculations to follow the mixing process via ex-situ 4D micro-CT measurements. A two-phase granular mixture was used for this purpose. The effect of container size on the mixing process was investigated. Our systems were simple enough that it was possible to closely model them with simulations, thus the experimental results could be compared with simulated ones acquired via DEM calculations. To the best of our knowledge, lacunarity has not yet been used to describe the mixing process for real 3D micro-CT datasets or to compare simulated and experimental data.

Although improvements can always be made in every process and mixing is no exception, improving the mixing process is not the aim of this work. Our main objective was to bring the attention of the scientific community to the opportunities the micro-CT technique provides in the field of mixing and to offer an easy-to-use, robust tool to quantify the progress of mixing. Thus, we chose a fairly simple model mixing experiment to demonstrate the great opportunities that lie within micro-CT imaging and lacunarity calculations.

Materials and methods

The experimental setup for the mixing tests was quite simple. The setup was optimized for micro-CT investigations and lacunarity calculations. Thus, the 3D-printed containers were made of polylactic acid, which have a low X-ray attenuation coefficient,

and the two components of the mixture had highly different attenuation coefficients; ca. 500 calcium–alginate beads (with an average density of 1.2 g/cm^3 and an average diameter of 1.75 mm) were mixed with ca. 5000 polystyrene spheres (with an average density of 1.05 g/cm^3 and an average diameter of 1.1 mm). For each experiment, equal amounts of particles were used for better comparability. No mixing fins were used inside the containers for easier imaging. Three different container sizes were used for the experiments with 20 × 20 × 25 mm^3, 20 × 20 × 35 mm^3 and 20 × 20 × 40 mm^3 inner volumes. The shape of the container was chosen to fit our lacunarity calculation algorithm. For better reproducibility, a precision stepper motor was used for the mixing process. One mixing cycle means a complete 360° turn around the cross-axis (Fig.1a). The containers were rotated for 10 cycles and at the beginning and after 1, 2, 3, 5, 7 and 10 cycles, micro-CT measurements were conducted.

Micro-CT images were taken using a Bruker Skyscan 2211 nanotomograph (Skyscan, Bruker, Belgium) using 100 kV source voltage, 270 μA current and 40 ms exposure time. The images were taken at 25-μm pixel resolution in microfocus mode. The samples were rotated at 180° with 0.2° angular size and a total of 1042 X-ray shadow projections were collected. The rotation step size was small enough that the movement between image acquisitions does not cause any additional mixing of the particles. The measurement setup is shown in Fig. 1b. The 3D images were reconstructed using NRecon Reconstruction Software (Skyscan, Bruker, Belgium) during which the most commonly occurring imaging artifacts were corrected. For the image post-processing and visualization, CTAn and CTVox software packages (Skyscan, Bruker, Belgium) were used.

In Fig. 1b, the volume rendered 3D micro-CT image shows both the calcium–alginate and the polystyrene particles. After image post-processing and segmentation, for better visibility, only the calcium–alginate beads are shown, and hereinafter only these beads are presented on the micro-CT images. All the lacunarity calculations were carried out on binary images only

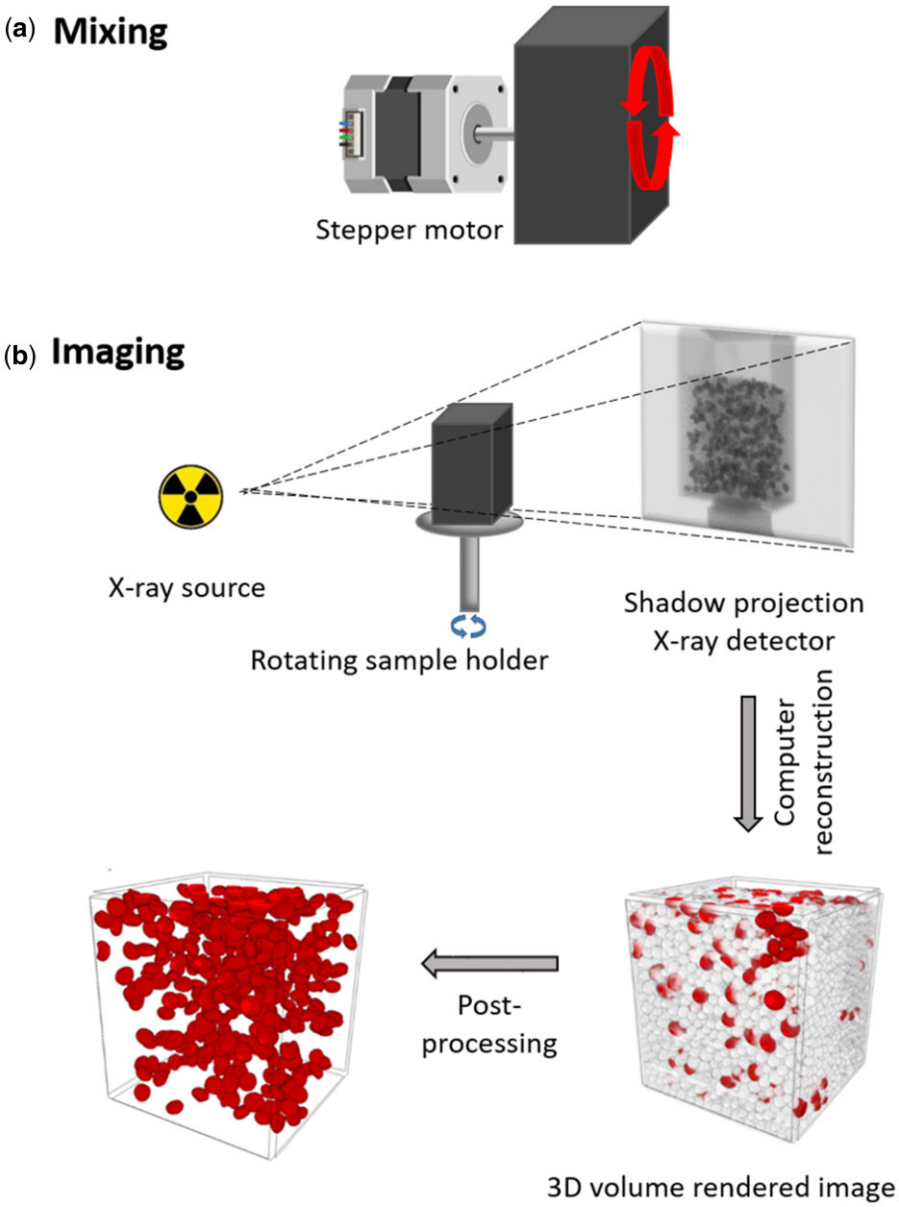

Figure 1. Schematic representation of the (a) mixing and the (b) micro-CT imaging process.

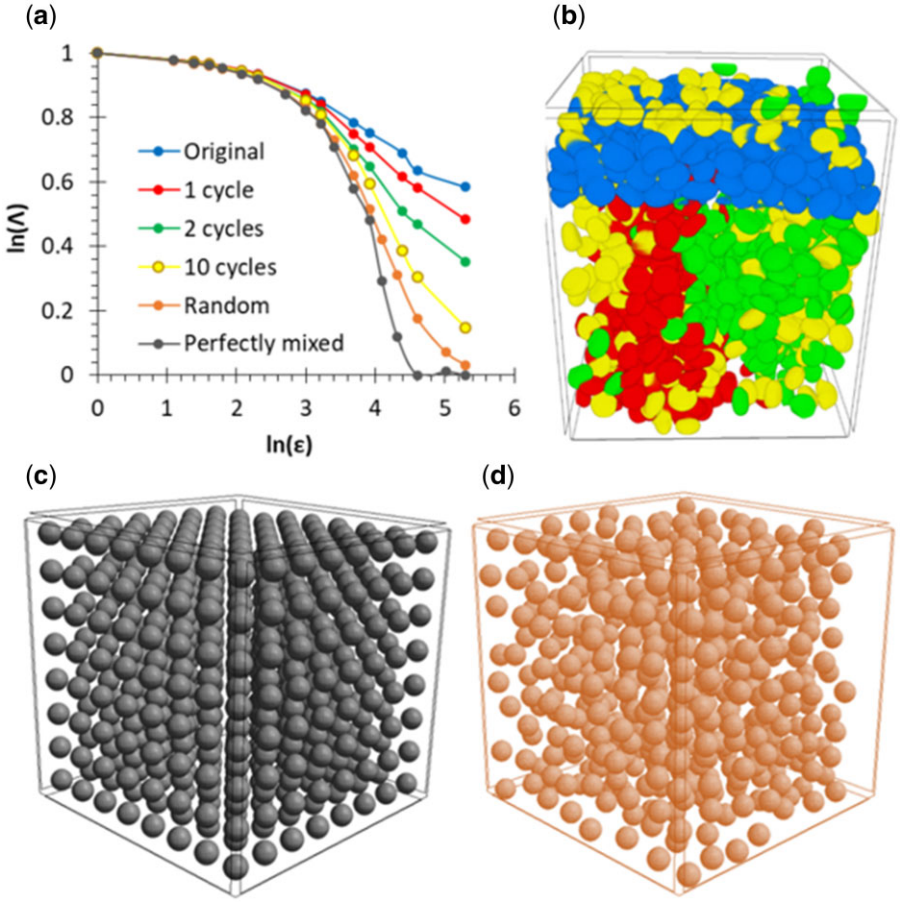

Figure 2. Lacunarity curves (a) and the corresponding 3D-rendered micro-CT images (b–d) of different stages of the mixing process—experimental results (b) at the beginning (blue) and after 1 (red), 2 (green) and 10 (yellow) mixing cycles for the medium container size, and simulated results for a cubically ordered (c, dark gray) and a nonoverlapping random (d, orange) dataset.

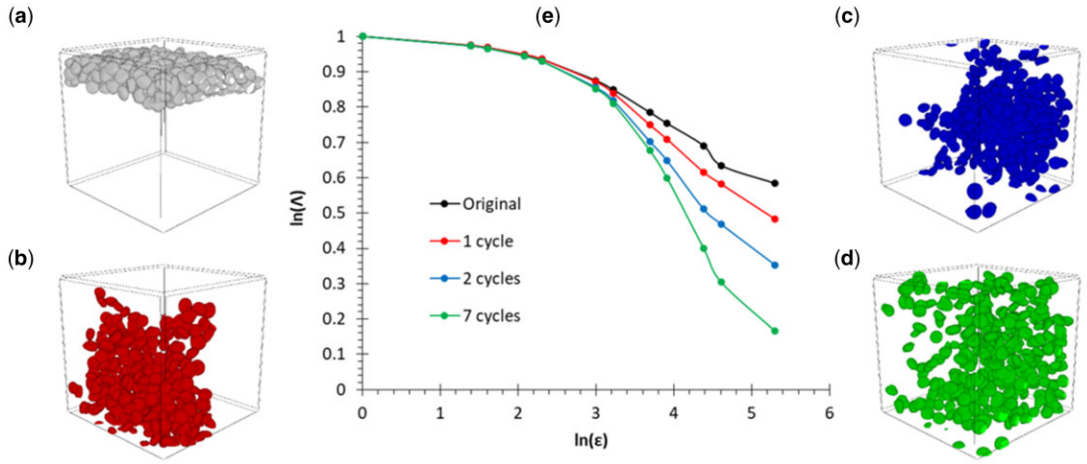

Figure 3. Micro-CT images of the same sample at the beginning (a) and after 1 (b), 2 (c),and 7 (d) mixing cycles and their corresponding lacunarity curves (e).

containing the positions of the calcium–alginate particles. Lacunarity calculations were conducted using our own software Lac3D [24] that uses an FGM. The lacunarity values were normalized for better comparability. Simulated datasets (cubic, non-overlapping random) were generated using a self-developed software.

DEM simulations were implemented using the LIGGGHTS [70] general granular simulation software. The DEM algorithm resolves the particle–particle interactions and integrates both the translational and rotational motion of each particle. The interaction force between the two contacting particles was computed via the Hertz model. This scheme allows the estimation of the

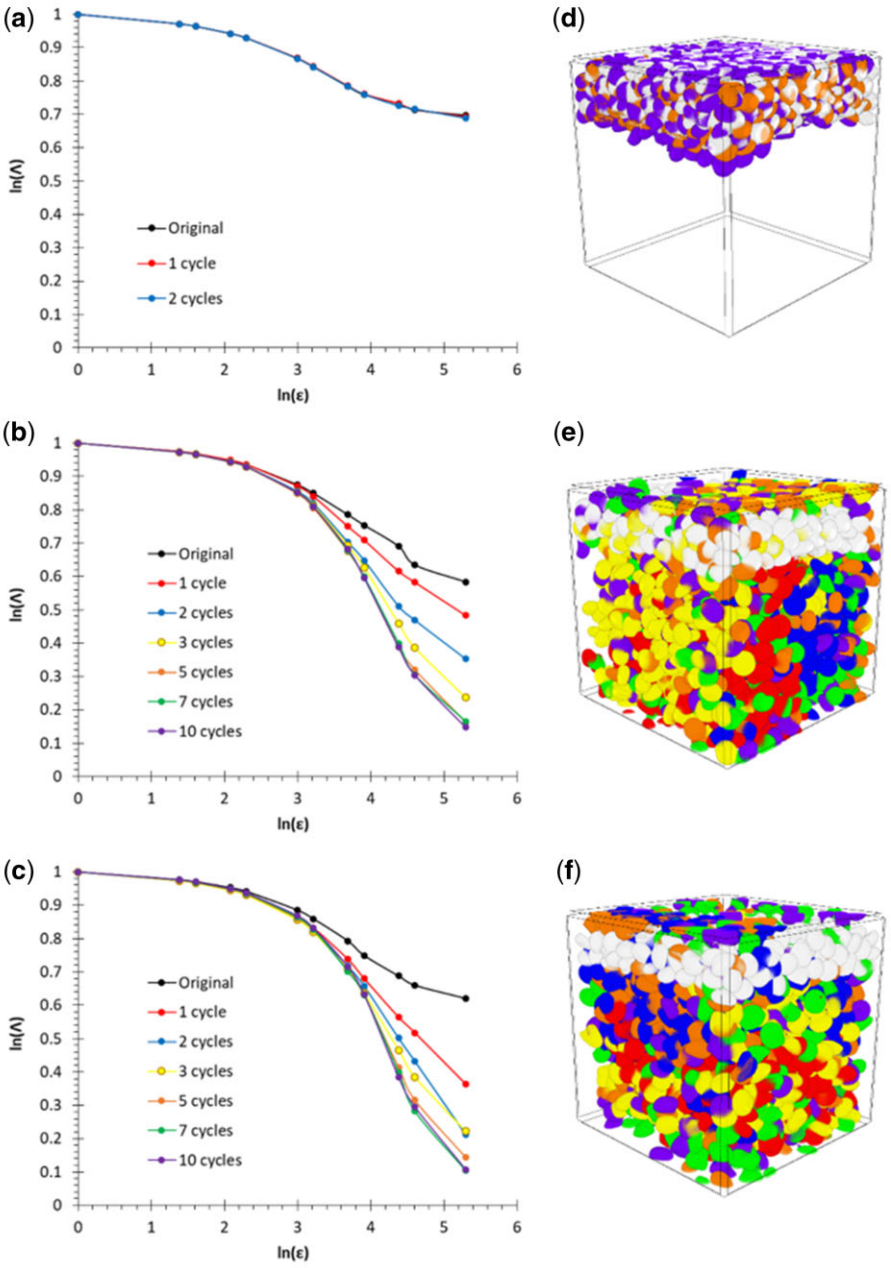

Figure 4. The lacunarity curves (a–c) of the three different systems and their corresponding 3D-rendered micro-CT images (d–f) for the smallest (a and d; 20 × 20 × 25 mm^3, the medium (b and e; 20 × 20 × 35 mm^3) and the largest (c and f; 20 × 20 × 40 mm^3) container, at the beginning (black) and after 1 (red), 2 (blue), 3 (yellow), 5 (orange), 7 (green) and 10 (purple) mixing cycles.

following elastic and damping interaction parameters: Young modulus (Y_m), Poisson's ratio (ν) of the material, the restitution coefficient (e) and friction coefficient (μ) of the particles. In our simulations, we used the following values: $Y_m = 5 \times 10^6$ Pa, $\nu = 0.45$, $e = 0.2$ and $\mu = 0.5$.

We used cells with closed boundaries with sizes 20 × 20 × 35 mm^3 and 20 × 20 × 40 mm^3 filled with a two-component mixture of spherical particles. The mixture consisted of 5000 particles with a diameter of 1.1 mm and density of 1.05 g/cm^3 and 500 particles with a diameter of 1.75 mm and density of 1.2 g/cm^3. To create the initial configuration of particles, they were placed randomly in a container much higher than the simulated cell size (the other dimensions were the same) with the larger particles on the top. Then the particles were released to fall due to gravity. We then used the relaxed state of this mixture to simulate the mixing process. To mimic the mixing process, we rotated the container by defining the rotation axis and the period of rotation. As the DEM method provides the trajectory of each particle, lacunarity calculations can be done at any desired state of the system.

Results and discussion

Lacunarity is a lesser-known measure of spatial heterogeneity, which can be used for the quantitative description of mixing. In Fig. 2, the lacunarity curves of a mixing process are compared to

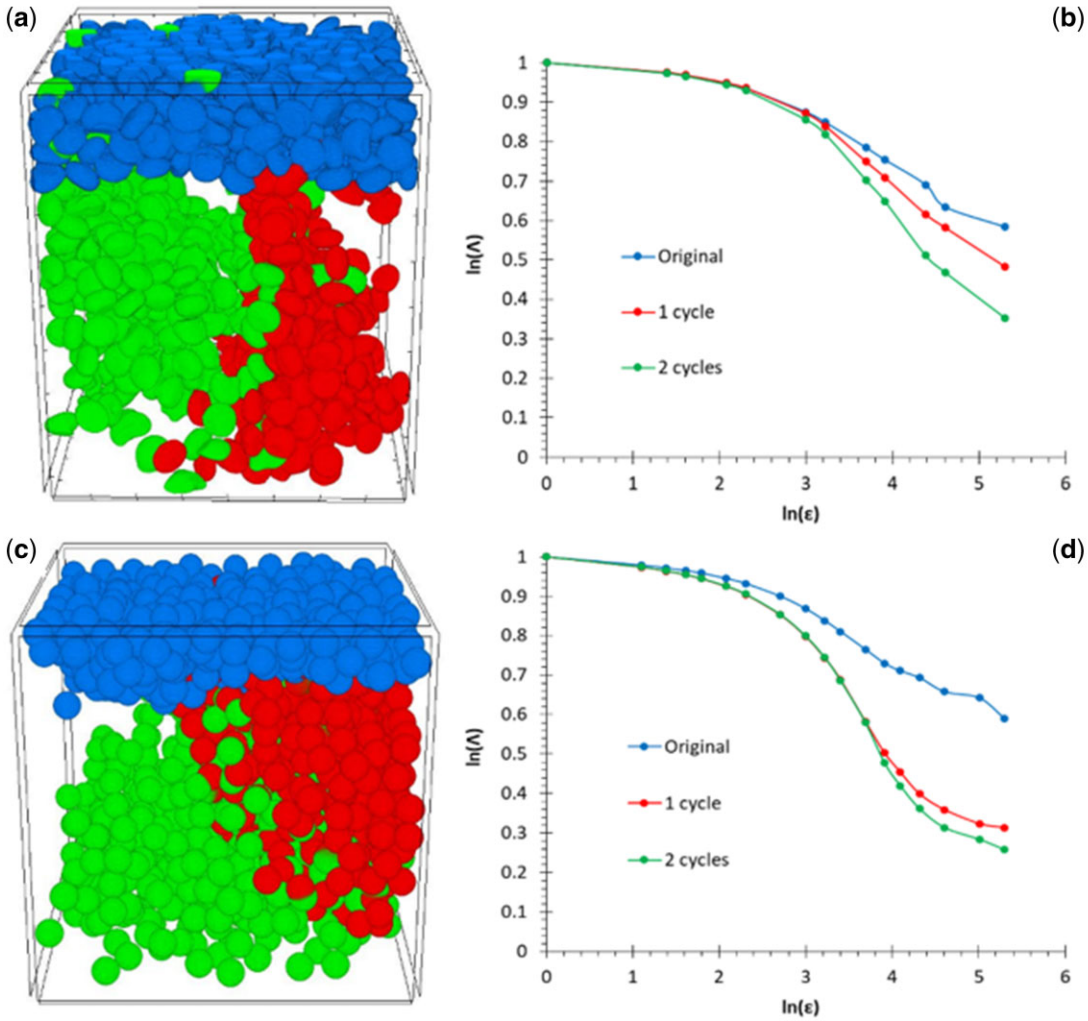

Figure 5. Comparison of the experimental (a and b) and simulated (c and d) lacunarity curves (b and d) and the 3D-rendered micro-CT images (a and c) for the medium-sized container.

the curves of the two simulated datasets (Fig. 2a). For the experimental part, four different stages of mixing are represented with their lacunarity curves and corresponding micro-CT images (Fig. 2b), showing a mixing process from the beginning to the completely mixed state (the most homogeneous state achievable in our specific mixing experiment). The simulated datasets represent a cubically ordered (Fig. 2c) and a non-overlapping random (Fig. 2d) layout. The differences in the corresponding lacunarity curves are clearly visible. The higher the lacunarity values, the more heterogeneous the system. With growing box sizes, the homogeneity improves. As expected, the most heterogeneous curve corresponds to the starting position of the mixing experiment, and as the mixing process progresses, the lacunarity values decrease. The non-overlapping random and the cubic layouts were the most homogeneous, and at bigger box sizes, they were completely homogeneous according to the lacunarity curves. The two corresponding lacunarity curves are shaped relatively similar to each other. In the case of the completely mixed stage, the lacunarity curve indicates a considerably more heterogeneous state due to the non-ideal nature of experimental setups. The shape of the lacunarity curves also bears great significance. All the curves are practically the same until a certain box size is reached, and it is the one comparable in size with the particle size. After that point, the real differences between each stage can be seen as the curves separate.

The importance of showing lacunarity as a function as opposed to a single value can also be easily comprehended from this example; if values at small box sizes are chosen for the comparison, no difference can be seen between the stages, while with increasing box size the difference also increases. In Fig. 3, the results of one of the mixing experiments in the medium-sized container can be seen. The presented micro-CT images (Fig. 3a–d) proved that a mere qualitative analysis of the mixtures does not give sufficient information regarding the state of the mixing. From these images, the difference between the stages cannot be properly apprehended. The respective lacunarity curves (Fig. 3e), however, perfectly demonstrate the homogenization of the mixture over time. As can be expected, with the increasing number of mixing cycles, the mixture becomes more homogeneous. The curves are similarly shaped for each stage, and the smallest lacunarity value was reached after seven mixing cycles.

The mixing experiments were carried out for all three container sizes to show that lacunarity can reliably show the difference between various systems. The results can be seen in Fig. 4. The experiments yielded the anticipated results. In the smallest container (Fig. 4a and d), there was practically no room for

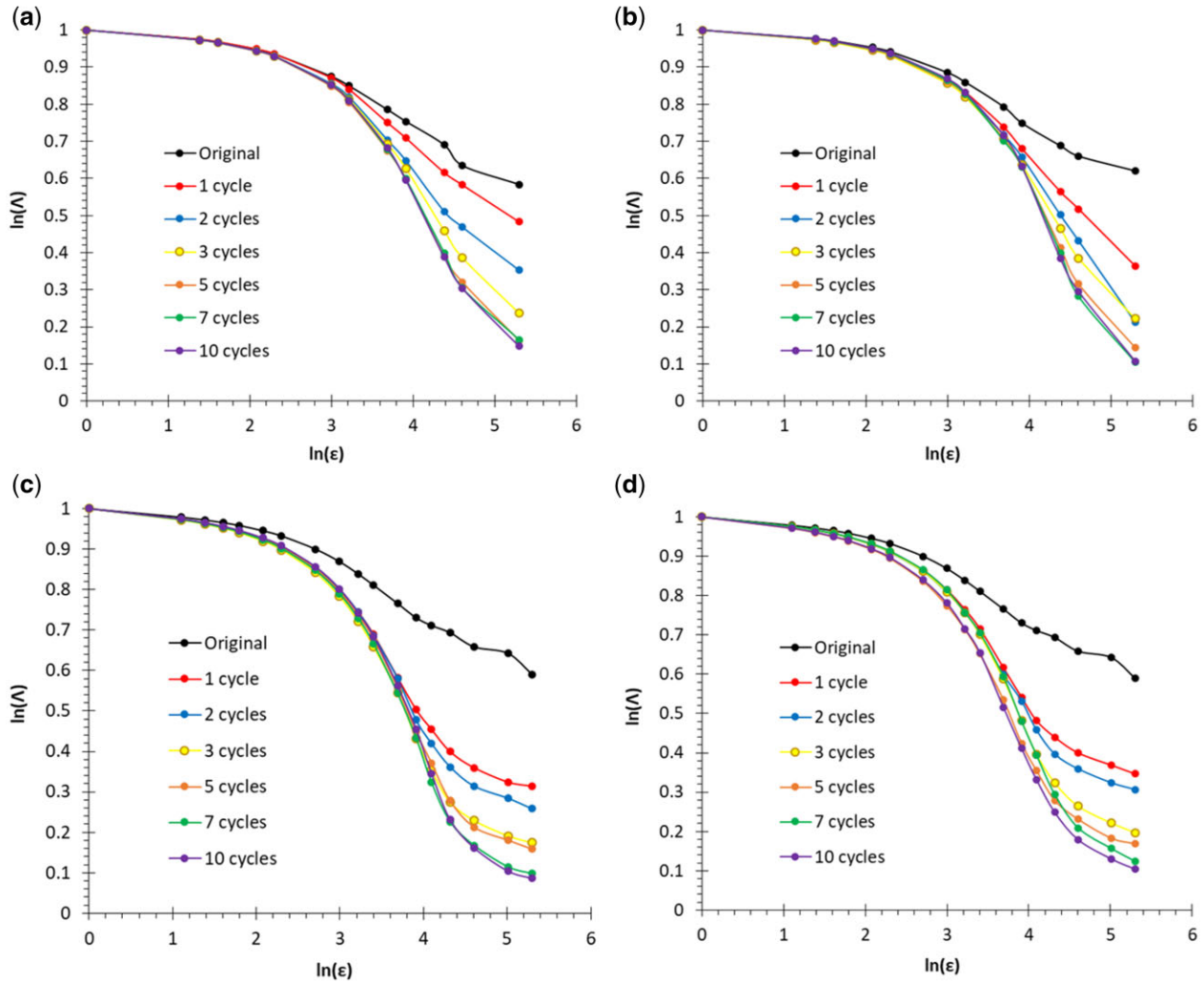

Figure 6. Lacunarity curves of the experimental (a and b) and simulated (c and d) datasets for the medium (a and c) and the largest (b and d) box sizes.

mixing, thus there is no real difference between the different stages. This can be seen either on the provided micro-CT images or the corresponding lacunarity curves. The different stages of mixing are illustrated with different colors for each experiment. For the smallest container size, the different stages overlap, and there is no mixing between the two components. The corresponding lacunarity curves also overlap, which provides further proof of the reliability of lacunarity calculations. For the other two container sizes, the visualization is not enough to show the differences between the stages. The lacunarity curves, however, show great differences between the stages. For both samples, a continuous homogenization of the components can be observed, until reaching the most homogeneous state for the given system. Unsurprisingly, in the case of the largest container size (Fig. 4c and f), the mixing is faster and more efficient than for the medium-sized container (Fig. 4b and e). Although, after seven mixing cycles no further homogenization was observed for either sample. At the end of the experiments for the largest box size, the lacunarity values were 0.688 for the smallest, 0.148 for the medium and 0.108 for the largest container. A completely homogeneous state cannot be reached by this experiment due to its imperfections; for instance, the nonideal shape and size distributions of the particles, the difference in densities and the shape of the container.

Afterward, the experimental results were compared with simulated datasets; the results are shown in Figs 5 and 6. Simulations were only conducted for the medium and the largest container sizes because of the failed mixing experiment with the smallest container. In Fig. 5, the micro-CT images (Fig. 5a and c) and lacunarity curves (Fig. 5b and d) of the medium container size are represented. They have shown great similarities, thus proving the applicability of simulations to complement or even substitute real-life experiments in the future. The visual representation and the lacunarity curves both show great resemblance. In the case of the simulated samples, a more homogeneous state could be reached, compared to the experimental results, due to their ideal nature (completely spherical particles, uniform particle size, no environmental effects). The shapes of the lacunarity curves are similar. The lacunarity at the beginning for the biggest box size was 0.57 for the experimental and 0.59 for the simulated data. After two mixing cycles, these values decreased to 0.353 and 0.307, respectively.

Figure 6 shows the results of the entire experiments for both container sizes. In the case of the medium container size (Fig. 6a and c), the final lacunarity values at the largest box size are 0.148 and 0.104 for the experimental and simulated datasets, respectively. For the largest container sizes (Fig. 6b and d), these values are 0.108 and 0.086, respectively. The differences are clearly

visible, but not excessive, and the same trends can be observed, thus proving the usefulness of the simulations. It is anticipated that with further fine-tuning of the simulating algorithm, the simulated results could approximate the experimental data even more closely.

Conclusions

In this work, the applicability of micro-CT measurements and lacunarity calculations were examined for the investigation of the mixing process of granular materials. We were the first to calculate the 3D lacunarity of mixtures. While a huge amount of studies about mixing indices only used simulated data, we quantified the mixing process for real-life 3D micro-CT datasets. According to our results, micro-CT is a highly capable device to investigate mixing in appropriate systems qualitatively and quantitatively. Lacunarity appeared to be an appropriate and easy-to-use tool to quantify mixing efficiency. As opposed to traditional mixing indices, lacunarity curves bear additional significance. The effect of container size on the mixing process was also investigated and an improvement in the homogenization process was observed with increasing container size. For our given system, the most homogeneous state was reached after seven mixing cycles; further mixing did not improve the homogeneity of the mixture. As lacunarity calculations can easily be conducted on simulated datasets, according to our results, it also enables the comparison of simulations with real-life experiments, which in the future can even be replaced by simulations. Simulations resulted in more homogeneous mixtures compared to the experiments due to their ideal nature, but the experimental and simulated results are comparable.

Data availability

The data underlying this article will be shared on reasonable request to the corresponding author.

Author Contributions

Lívia Vásárhelyi (Investigation [equal], Writing—original draft [equal]), Daniel Sebők (Conceptualization [equal], Software [equal], Writing—original draft [equal]), Imre Szenti (Investigation [equal]), Ádám Tóth (Investigation [equal]), Sára Lévay (Investigation [supporting], Software [equal]), Robert Vajtai (Supervision [equal]), Zoltán Kónya (Supervision [equal]) and Akos Kukovecz (Conceptualization [equal], Supervision [lead], Writing—review and editing [equal]).

Funding

Project no. TKP2021-NVA-19 has been implemented with the support provided by the Ministry of Innovation and Technology of Hungary from the National Research, Development and Innovation Fund, financed under the TKP2021-NVA funding scheme.

Conflict of interest statement: None declared.

References

1. Cullen P, Bakalis S, Sullivan C. Advances in control of food mixing operations. *Curr Opin Food Sci* 2017;**17**:89–93.
2. Gijón-Arreortúa I, Tecante A. Mixing time and power consumption during blending of cohesive food powders with a horizontal helical double-ribbon impeller. *J Food Eng* 2015;**149**:144–52.
3. Lerch JO, Bester HL, Van Rooyen AS *et al.* The effect of mixing on the performance of macro synthetic fibre reinforced concrete, *Cem Concr Res* 2018;**103**:130–139.
4. Elaqra HA, Haloub MAA, Rustom RN. Effect of new mixing method of glass powder as cement replacement on mechanical behavior of concrete. *Constr Build Mater* 2019;**203**:75–82.
5. Sarkar M, Sharmin YM. Improving the drug dissolution profile of poorly aqueous soluble lovastatin using hydrophilic polymers by solid dispersion and physical mixing techniques. *Natl J Physiol Pharm Pharmacol* 2020;**11**:1.
6. Peterwitz M, Schembecker G. Evaluating the potential for optimization of axial back-mixing in continuous pharmaceutical manufacturing. *Comput Chem Eng* 2021;**147**:107251.
7. Kim KM, Oh HM, Lee JH. Controlling the emulsion stability of cosmetics through shear mixing process. *Korea Aust Rheol J* 2020;**32**:243–9.
8. Lappan U, Naas C, Scheler U. Influence of the mixing ratio on the dynamics of polymer segments in polyelectrolyte complexes. *Macromol Chem Phys* 2021;**222**:2000445.
9. Reddy LPB, Prakash HGR, Ravikiran YT *et al.* Structural and humidity sensing properties of niobium pentoxide-mixed nickel ferrite prepared by mechano-chemical mixing method, *J Mater Sci Mater Electron* **31**:2020;21981–99.
10. Bánfai B, Ganzler K, Kemény S. Content uniformity and assay requirements in current regulations. *J Chromatogr A* 2007;**1156**:206–12.
11. Portillo PM, Ierapetritou MG, Muzzio FJ. Characterization of continuous convective powder mixing processes. *Powder Technol* 2008;**182**:368–78.
12. Ottino JM, Khakhar DV. Mixing and segregation of granular materials. *Annu Rev Fluid Mech* 2000;**32**:55–91.
13. Schröter M, Ulrich S, Kreft J *et al.* Mechanisms in the size segregation of a binary granular mixture. *Phys. Rev E* 2006;**74**:011307.
14. Jain N, Ottino JM, Lueptow RM. Regimes of segregation and mixing in combined size and density granular systems: an experimental study. *Granul Matter* 2005;**7**:69–81.
15. Nadeem H, Heindel TJ. Review of noninvasive methods to characterize granular mixing. *Powder Technol* 2018;**332**:331–50.
16. Porion P, Sommier N, Faugère A-M *et al.* Dynamics of size segregation and mixing of granular materials in a 3D-blender by NMR imaging investigation. *Powder Technol* 2004;**141**:55–68.
17. Finger T, von Rüling F, Lévay F *et al.* Segregation of granular mixtures in a spherical tumbler. *Phys Rev E* 2016;**93**:032903.
18. McCarthy JJ, Khakhar DV, Ottino JM. Computational studies of granular mixing. *Powder Technol* 2000;**109**:72–82.
19. McCarthy JJ, Shinbrot T, Metcalfe G *et al.* Mixing of granular materials in slowly rotated containers. *AIChE J* 1996;**42**:3351–63
20. Bridgwater J. Mixing of powders and granular materials by mechanical means—A perspective. *Particuology* 2012;**10**:397–427.
21. Bertrand F, Leclaire L-A, Levecque G. DEM-based models for the mixing of granular materials. *Chem Eng Sci* 2005;**60**:2517–31.
22. Hounsfield GN. Computerized transverse axial scanning (tomography): Part I: *Description of system. Br J Radiol* 1973;**46**:1016–22.
23. Elliott JC, Dover SD. X-ray microtomography. *J Microsc* 1982;**126**:211–3.
24. Vásárhelyi L, Kónya Z, Kukovecz Á *et al.* Microcomputed tomography–based characterization of advanced materials: a review. *Mater Today Adv* 2020;**8**:100084.

25. Salvo L, Suéry M, Marmottant A *et al.* 3D imaging in material science: Application of X-ray tomography. *Comptes Rendus Phys* 2010;**11**:641–9.
26. Asachi M, Nourafkan E, Hassanpour A. A review of current techniques for the evaluation of powder mixing. *Adv Powder Technol* 2018;**29**:1525–49.
27. Poutiainen S, Pajander J, Savolainen A *et al.* Evolution of granule structure and drug content during fluidized bed granulation by X-ray microtomography and confocal Raman spectroscopy. *J Pharm Sci* 2011;**100**:5254–69.
28. Liu R, Yin X, Li H *et al.* Visualization and quantitative profiling of mixing and segregation of granules using synchrotron radiation X-ray microtomography and three dimensional reconstruction. *Int J Pharm* 2013;**445**:125–33.
29. Mandelbrot BB. *The Fractal Geometry of Nature*. San Francisco: Freeman, 1982.
30. Plotnick RE, Gardner RH, Hargrove WW *et al.* Lacunarity analysis: A general technique for the analysis of spatial patterns. *Phys Rev E* 1996;**53**:5461–8.
31. Roy A, Perfect E, Dunne WM *et al.* A technique for revealing scale-dependent patterns in fracture spacing data. *J Geophys Res Solid Earth* 2014;**119**:5979–86.
32. Nichita MV, Paun MA, Paun VA *et al.* Fractal analysis of brain glial cells. *Fractal dimension and lacunarity, UPB Sci Bull Ser A Appl Math Phys* 2019;**81**:273–84.
33. Waliszewski P. The quantitative criteria based on the fractal dimensions, entropy, and lacunarity for the spatial distribution of cancer cell nuclei enable identification of low or high aggressive prostate carcinomas. *Front Physiol* 2016;**7**:1–16.
34. Palanivel DA, Natarajan S, Gopalakrishnan S *et al.* Multifractal-based lacunarity analysis of trabecular bone in radiography. *Comput Biol Med* 2020;**116**:103559.
35. N'Diaye M, Degeratu C, Bouler JM *et al.* Biomaterial porosity determined by fractal dimensions, succolarity and lacunarity on microcomputed tomographic images. *Mater Sci Eng C* 2013;**33**:2025–30.
36. Massai D, Pennella F, Gentile P *et al.* Image-based three-dimensional analysis to characterize the texture of porous scaffolds. *Biomed Res Int* 2014;**2014**:1–8.
37. Xia Y, Cai J, Perfect E *et al.* Fractal dimension, lacunarity and succolarity analyses on CT images of reservoir rocks for permeability prediction. *J Hydrol* 2019;**579**:124198.
38. Dos Santos CR, Antonino ACD, Heck RJ *et al.* 3D soil void space lacunarity as an index of degradation after land use change. *Acta Sci - Agron* 2020;**42**:1–9.
39. Liu K, Ostadhassan M. Quantification of the microstructures of Bakken shale reservoirs using multi-fractal and lacunarity analysis. *J Nat Gas Sci Eng* 2017;**39**:62–71.
40. Liu Y, Jeng D-S. Pore structure of grain-size fractal granular material. *Materials (Basel)* 2019; **12**:2053
41. Pennella F, Rossi M, Ripandelli S *et al.* Numerical and experimental characterization of a novel modular passive micromixer. *Biomed Microdevices* 2012;**14**:849–62.
42. Allain C, Cloitre M. Characterizing the lacunarity of random and deterministic fractal sets. *Phys Rev A* 1991;**44**:3552–8.
43. Hanen A, Imen B, Asma BA *et al.* Multifractal modelling and 3D lacunarity analysis. *Phys Lett Sect A Gen At Solid State Phys* 2009;**373**:3604–9.
44. Sebők D, Vásárhelyi L, Szenti I *et al.* Fast and accurate lacunarity calculation for large 3D micro-CT datasets. *Acta Mater* 2021;**214**:116970.
45. Cousins TA, Ghanbarian B, Daigle H. Three-dimensional lattice boltzmann simulations of single-phase permeability in random fractal porous media with rough pore–solid interface. *Transp Porous Media* 2018;**122**:527–46.
46. Govender N, Wilke DN, Wu CY *et al.* Large-scale GPU based DEM modeling of mixing using irregularly shaped particles. *Adv Powder Technol* 2018;**29**:2476–90.
47. Saeed MK, Siraj MS. Mixing study of non-spherical particles using DEM. *Powder Technol* 2019;**344**:617–27.
48. Jin X, Chandratilleke GR, Wang S *et al.* DEM investigation of mixing indices in a ribbon mixer. *Particuology* 2021;**60**:37–47.
49. Zuo Z, Gong S, Xie G *et al.* DEM simulation of binary mixing particles with different density in an intensive mixer. *Powder Technol* 2021;**383**:454–70.
50. Tsunazawa Y, Soma N, Sakai M. DEM study on identification of mixing mechanisms in a pot blender. *Adv Powder Technol* 2022;**33**:103337.
51. Li S, Kajiwara S, Sakai M. Numerical investigation on the mixing mechanism in a cross-torus paddle mixer using the DEM-CFD method. *Powder Technol* 2021;**377**:89–102.
52. Chandratilleke GR, Yu AB, Bridgwater J. A DEM study of the mixing of particles induced by a flat blade. *Chem Eng Sci* 2012;**79**:54–74.
53. Soni RK, Mohanty R, Mohanty S *et al.* Numerical analysis of mixing of particles in drum mixers using DEM. *Adv Powder Technol* 2016;**27**:531–40.
54. Liu X, Hu Z, Wu W *et al.* DEM study on the surface mixing and whole mixing of granular materials in rotary drums. *Powder Technol* 2017;**315**:438–44
55. Lévay S, Fischer D, Stannarius R *et al.* Interacting jammed granular systems. *Phys Rev E* 2021;**103**:042901
56. Lévay S., Fischer D, Stannarius R *et al.* Frustrated packing in a granular system under geometrical confinement. *Soft Matter* 2018;**14**:396–404.
57. Gui N, Yang X, Tu J *et al.* SIPHPM simulation and analysis of cubic particle mixing patterns and axial dispersion mechanisms in a three-dimensional cylinder. *Powder Technol* 2018;**335**:235–49.
58. Zhang Z, Gui N, Yang X *et al.* Discussion on the construction principle of new mixing indices and application for cubic particle mixing by SIPHPM. *Ind Eng Chem Res* 2020;**59**:19438–48.
59. Chandratilleke R, Yu A, Bridgwater J *et al.* Flow and mixing of cohesive particles in a vertical bladed mixer. *Ind Eng Chem Res* 2014;**53**:4119–30.
60. Deen NG, Willem G, Sander G *et al.* Numerical analysis of solids mixing in pressurized fluidized beds. *Ind Eng Chem Res* 2010;**49**:5246–53.
61. Lacey PMC. Developments in the theory of particle mixing. *J Appl Chem* 2007;**4**:257–68.
62. Siiriä S, Yliruusi J. Determining a value for mixing: mixing degree. *Powder Technol* 2009;**196**:309–17.
63. Wen Y, Liu M, Liu B *et al.* Comparative study on the characterization method of particle mixing index using DEM method. *Procedia Eng* 2015;**102**:1630–42.
64. Cho M, Dutta P, Shim J. A non-sampling mixing index for multi-component mixtures. *Powder Technol* 2017;**319**:434–44.
65. Lacey PMC. The mixing of solid particles. *Chem Eng Res Des* 1997;**75**:S49–55.
66. Feng YQ, Xu BH, Zhang SJ *et al.* Discrete particle simulation of gas fluidization of particle mixtures. *AIChE J* 2004;**50**:1713–28.

67. Asmar BN, Langston PA, Matchett AJ. A generalised mixing index in distinct element method simulation of vibrated particulate beds. *Granul Matter* 2002;**4**:129–38.
68. Siraj MS, Radl S, Glasser BJ *et al.* Effect of blade angle and particle size on powder mixing performance in a rectangular box. *Powder Technol* 2011;**211**:100–13.
69. Chandratilleke GR, Yu AB, Bridgwater J *et al.* A particle-scale index in the quantification of mixing of particles. *AIChE J* 2012;**58**:1099–118.
70. Kloss C, Goniva C, Hager A *et al.* Models, algorithms and validation for opensource DEM and CFD-DEM. *Prog Comput Fluid Dyn An Int J* 2012;**12**:140.